Supporting Information

A General Doping Rule: Rational Design of Ir-doped Catalysts for Oxygen Evolution Reaction

Chuan Zhou,[a] Haiyang Yuan,[a] P. Hu,[ab] Haifeng Wang[a,*]

[a]Key Laboratory for Advanced Materials, Research Institute of Industrial Catalysis and Centre for Computational Chemistry, East China University of Science and Technology, Shanghai 200237, China

[b]School of Chemistry and Chemical Engineering, The Queen's University of Belfast, Belfast BT9 5AG, U.K.

S1 Computational details

All the spin-polarized DFT calculations were performed with the Perdew−Burke−Ernzerhof (PBE) functional using the VASP,[1,2] in which the PAW method was applied to represent the core-valence electron interaction.[3] The valence electronic states were expanded in plane wave basis sets with energy cutoff at 450 eV. The (110) surfaces most exposed by rutile-type metal oxides (CrO_2, MnO_2, MoO_2, RuO_2, RhO_2, OsO_2 and IrO_2) were modeled as a *p*(2×1) periodic slab with four layers, thus 1/2 monolayer surface doping can be observed. The bottom two layers are fixed, and all other atoms are fully relaxed. The vacuum layer is 20 Å. 4×4×1 k-point mesh was used for these surface slabs. For the bulk structure, 5×5×7 k-point mesh was used. The force threshold for the optimization was 0.05 eV/Å. Here the DFT+U approach was used to treat the electronic correlation in the localized *d*-orbital of Mn with the U value of 1.6,[4] and an antiferromagnetic helical spin arrangement for β-MnO_2 was imposed in our calculation.[5] The adsorption energies were calculated with the following equation:

$$E_{ads} = E(_{adsorbate/oxide}) - E(_{oxide}) - E(_{adsorbate}) \quad (1)$$

where adsorbates denote the surface species such as O and H. With this definition, a more negative value of adsorption energy suggests the stronger adsorption.

S2 Scaling behaviors for adsorbates on doped rutile-type TMOs

In this work the adsorption behaviors of atomic H and O, two independent descriptors of the common adsorbates as revealed in our previous work, are studied on rutile-type TMOs including CrO_2, MnO_2, MoO_2, RuO_2, RhO_2, OsO_2 and IrO_2 and their doped counterparts inside each other, in pursuit of the adsorption tuning rule of dopants by examining two typical doping modes.

Table S1. The adsorption energies of atomic O and H on doped rutile-type TMOs. R^2 is the correlation coefficient of scaling relation between $E_{H@M(G)}$ and $E_{O@M(G)}$, G represents the doped element.

Guest element	Host element	$E_{H@M(G)}$	$E_{O@M(G)}$	R^2
Cr	Cr	-1.03	-4.18	0.85
	Mn	-0.49	-3.57	
	Mo	-1.84	-4.78	
	Ru	-1.06	-4.07	
	Rh	-0.92	-3.69	
	Os	-1.42	-4.44	
	Ir	-1.30	-3.98	
Mn	Cr	-1.58	-3.37	0.67
	Mn	-1.20	-2.39	
	Mo	-1.54	-3.19	
	Ru	-1.23	-2.94	
	Rh	-1.20	-2.47	
	Os	-1.38	-3.32	
	Ir	-1.35	-2.69	
Mo	Cr	-1.19	-5.32	0.87
	Mn	-0.81	-4.46	
	Mo	-2.02	-6.33	
	Ru	-1.32	-5.00	
	Rh	-1.15	-4.48	
	Os	-1.71	-5.87	
	Ir	-1.67	-5.51	
Ru	Cr	-2.08	-4.26	0.81
	Mn	-1.84	-4.29	
	Mo	-2.70	-4.67	
	Ru	-1.96	-4.22	
	Rh	-1.87	-4.10	
	Os	-2.20	-4.51	
	Ir	-2.20	-4.45	
Rh	Cr	-2.50	-3.42	0.92
	Mn	-2.15	-3.13	
	Mo	-2.73	-3.60	
	Ru	-2.25	-3.32	
	Rh	-2.23	-3.21	

	Os	-2.46	-3.49	
	Ir	-2.59	-3.51	
Os	Cr	-2.53	-5.30074	0.70
	Mn	-2.06	-5.11029	
	Mo	-2.92	-5.40238	
	Ru	-2.50	-5.255	
	Rh	-2.32	-5.07917	
	Os	-2.81	-5.62	
	Ir	-2.76	-5.61642	
Ir	Cr	-3.00	4.36	0.80
	Mn	-2.59	4.31	
	Mo	-3.36	4.68	
	Ru	-2.83	4.27	
	Rh	-2.70	4.17	
	Os	-3.10	4.43	
	Ir	-3.14	4.46	

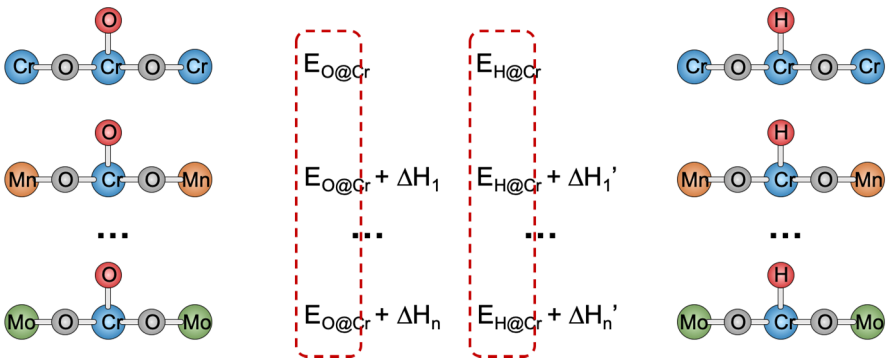

Fig. S1 A schematic diagram for explaining the linear correlations between $E_{O@M(Cr)}$ and $E_{H@M(Cr)}$.

Specifically, here we take the doping mode (ii) as illustration to give more details on the rationality of the correlation between $E_{H@M(Cr)}$ vector and $E_{O@M(Cr)}$ vector. Doping mode (ii) describes that one guest metal atom is doped in different host metal oxides. Fig. S1 illustrates the example of Cr doping in a series of rutile-type metal oxides. $E_{O@Cr}$ and $E_{H@Cr}$ are the adsorption energies of atomic O and H on the pristine CrO_2(110), respectively, while $E_{O@M(Cr)}$ and $E_{H@M(Cr)}$ are the adsorption energies of atomic O and H on the Cr site doped into different host oxides (MO_2(110)). Thus, $E_{O@M(Cr)}$-$E_{O@Cr}$ gives a vector [ΔH_1, ΔH_2, …, ΔH_n] describing the differences of O adsorption energy owing to the modulation of different host-regions on the Cr site, and the $E_{H@M(Cr)}$-$E_{H@Cr}$ vector (*i.e.* [ΔH_1', ΔH_2', …, ΔH_n']) describes the same case for the atomic H. For example, ΔH_1 and ΔH_1' correspond to the modulation effect of MnO_2 host on the Cr

site for the O and H adsorption, respectively, and is a relatively small item. Likewise, different host metals hold different ΔH_i (or ΔH_i') for O (or H) (i=1-n). Finally, for a specific G atom, the modulation effect of the host oxides on H and O binding strength is in the same trend and can be correlated with each other (see Figure 2d in the main text), which rationalize that $E_{H@M(Cr)}$ vector can correlate well with $E_{O@M(Cr)}$ vector accordingly.

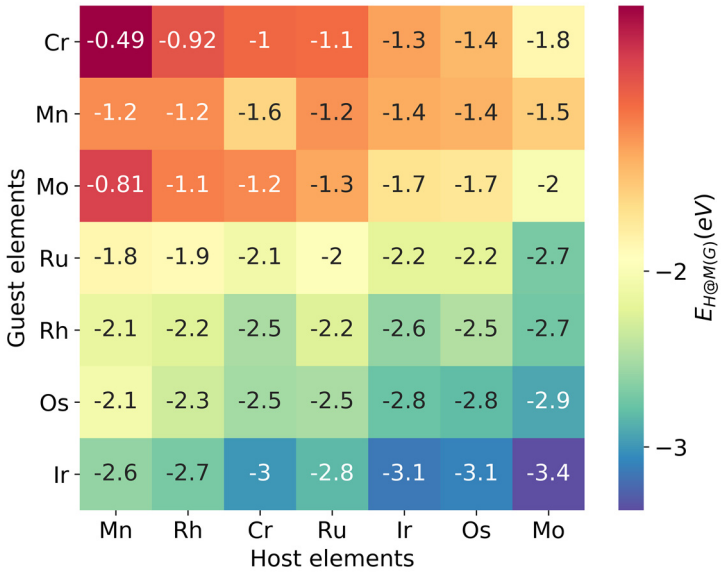

Fig. S2 Coutour plot of adsorption energies of atomic H on a series of doped rutile-type TMOs, which exhibits a range of (-3.4, -0.49) eV.

A systematic summarization of doping effect on tuning the adsorption energy of H is shown in Fig. S2. Notably, the adsorption trend of atomic H are different on undoped and doped rutile(110). According to the results of two doping modes in the main text, on doping mode (i), *i.e.* a specific host oxide with different guest atoms introduced, the adsorption energy of H on doped systems ($E_{H@M(G)}$) ranks in the order of G (G=Cr, Mn, Mo, Ru, Rh, Os and Ir): Cr < Mn < Mo < Ru < Rh < Os < Ir, which is consistent with the adsorption trend for H on pure rutile(110). However, a total different adsorption trend for H on doping mode (ii) can be observed. In this case, the same guest atom doped into different host oxides, thus making $E_{H@M(G)}$ ranks in the order of M (M=Mn, Rh, Cr, Ru, Ir, Os and Mo): Mn < Rh < Cr < Ru < Ir < Os < Mo, which is same to the adsorption trend for atomic O (see Fig. 3 in the main text). Despite of all these, to

improve the adsorption ability on a doped catalyst surface, one can adopt either host or guest metal with stronger binding ability.

S3 Calculation method for OER

To estimate and compare the activity trend of the oxygen evolution reaction (OER) on Ir active sites doped in different host TMO, the following common mechanism in acidic/neutral environment was considered[6-10]:

$$H_2O + * \rightarrow OH^* + H^+ + e \quad (1)$$

$$OH^* \rightarrow O^* + H^+ + e \quad (2)$$

$$H_2O + O^* \rightarrow OOH^* + H^+ + e \quad (3)$$

$$OOH^* \rightarrow O_2 + * + H^+ + e \quad (4)$$

where * represents the active site for OER, and OH*, O* and OOH* represent the adsorption of OH, O and OOH intermediates on the active site, respectively. Notably, the computational hydrogen electrode (CHE) model was used to present the chemical potentials of protons and electrons at any given pH and applied potential U, and thus the Gibbs free energy change ΔG_i of each step above (i = 1, 2, 3 and 4) can be written as:

$$\Delta G_1 = \Delta G_{OH} - eU \quad (5)$$

$$\Delta G_2 = \Delta G_O - \Delta G_{OH} - eU \quad (6)$$

$$\Delta G_3 = \Delta G_{OOH} - \Delta G_O - eU \quad (7)$$

$$\Delta G_4 = 4.92 - \Delta G_{OOH} - eU \quad (8)$$

where ΔG_O, ΔG_{OH} and ΔG_{OOH} are the Gibbs adsorption energies of O, OH and OOH on active centers and calculated relative to H_2O and H_2 at U = 0 V (vs U_{SHE}) and pH = 0. The sum of ΔG_{1-4} (4.92eV) is fixed to the negative of experimental Gibbs free energy of formation of two water molecules in order to avoid the calculation of the O_2 bond energy, which is difficult to determine accurately within GGA-DFT. U is the potential measured against standard hydrogen electrode (SHE) and was set to 0 V here.

Specifically, ΔG_O, ΔG_{OH}, and ΔG_{OOH} can be estimated according to $\Delta G_i = \Delta E_i + \Delta ZPE_i - T\Delta S_i$, with the zero point energy (ZPE) and entropy corrections included, while the energy differences ΔE_i can be calculated relative to H_2O and H_2 as

$$\Delta E_O = E(O^*) - E(*) - [E(H_2O) - E(H_2)] \quad (9)$$

$$\Delta E_{OH} = E(OH^*) - E(*) - [E(H_2O) - 1/2E(H_2)] \quad (10)$$

$$\Delta E_{OOH} = E(OOH^*) - E(*) - [2E(H_2O) - 3/2E(H_2)] \quad (11)$$

where $E(X^*)$ (X= O, OH, or OOH) are the total energies of X species adsorbed on the catalyst surface, while $E(H_2O)$ and $E(H_2)$ are the total energies of H_2O and H_2 in the gas phase. The more negative ΔE_X means the stronger adsorption of adsorbates on the surface.

Therefore, the theoretical overpotential (η) can be obtained from the Gibbs free energy change ΔG_i (i = 1, 2, 3 and 4) of each step above:

$$\eta = \max(\Delta G_1, \Delta G_2, \Delta G_3, \Delta G_4)/e - 1.23 \text{ [V]} \quad (12)$$

which can be used to assess the OER activity trend of Ir-based rutile-type TMO catalysts in acid/neutral environment. The obtained theoretical overpotentials of Ir active site with different other metal coordinated are summarized in Table S2.

Table S2. The detailed Gibbs free energy changes (ΔG_i, i = 1 to 4) of each step in OER and the relative overpotentials (η) on Ir activity center.

	Step *i*	IrO_2	Ir-CrO_2	Ir-MnO_2	Ir-MoO_2	Ir-RuO_2	Ir-RhO_2	Ir-OsO_2
ΔG_1	H_2O +* →OH* + e/H^+	0.03	0.07	0.39	-0.58	0.27	0.38	0.08
ΔG_2	OH* →O* + e/H^+	1.40	1.46	1.20	1.79	1.35	1.33	1.40
ΔG_3	H_2O + O* →OOH* + e/H^+	1.62	1.59	1.66	0.78	1.55	1.59	1.62
ΔG_4	OOH* →O_2 + * + e/H^+	1.87	1.80	1.67	2.93	1.74	1.61	1.88
	η	0.64	0.57	0.44	1.70	0.51	0.38	0.65

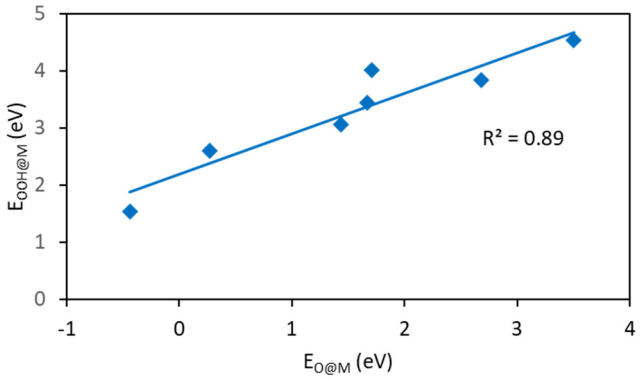

Figure S3. A scaling relation between adsorption energies of OOH* ($E_{OOH@M}$) and O adsorption energies ($E_{O@M}$) on the M_{cus} sites of rutile-type MO_2(110), where M=Cr, Mn, Mo, Ru, Rh and Os, respectively.

S4 The formation energies of doped rutile-type TMOs

The formation energy of doping process is defined with the following equation:

$$E_f = \gamma(A_{n-1}BO_{2n}) - (m-1)/m * \gamma(A_nO_{2n}) - 1/m * \gamma(B_nO_{2n}) \quad (13)$$

hereinto, m represents the number of surface metal atoms. For example, a $p(2\times1)$ periodic slab possesses 2 surface metal atoms, and a $p(4\times1)$ periodic slab has 4 surface metal atoms. $\gamma(A_{n-1}BO_{2n})$, $\gamma(A_nO_{2n})$ and $\gamma(B_nO_{2n})$ represent the surface energies of B-doped AO_2 surface, pure AO_2 surface and pure BO_2 surface, respectively, which can be expressed as follows:

$$\gamma(A_{n-1}BO_{2n}) = [E_{sur}(A_{n-1}BO_{2n}) - (\mathrm{n}-1)E(AO_2) - E(BO_2)]/2A_a \quad (14)$$

$$\gamma(A_nO_{2n}) = [E_{sur}(A_nO_{2n}) - \mathrm{n}E(AO_2)]/2A_a \quad (15)$$

$$\gamma(B_nO_{2n}) = [E_{sur}(B_nO_{2n}) - \mathrm{n}E(BO_2)]/2A_b \quad (16)$$

where $E_{sur}(A_{n-1}BO_{2n})$ is the total energies of the doped surfaces, while $E(AO_2)$ and $E(BO_2)$ are the average energies of AO_2 and BO_2 relative to their bulk phase, respectively. A_a and A_b represent the surface area. The formation energy explains the thermodynamic requirements for the formation of doped rutile(110); the more negative formation energy, the less prone to phase segregation in doped system. The formation energies of doped rutile-type transition metal oxides are shown in Table S3. Notably, Ir-doped MnO_2 and CrO_2 possess relatively low formation energies, which demonstrate that they can serve as the superior OER candidates.

Table S3. The formation energies of doped rutile-type transition metal oxides.

Dopant	Host oxides	E_f ($J\cdot m^{-2}$)	Dopant	Host oxides	E_f ($J\cdot m^{-2}$)
Cr	MnO_2	-0.18	Mn	CrO_2	0.40
	MoO_2	0.35		MoO_2	0.25
	RuO_2	0.27		RuO_2	0.36
	RhO_2	-0.15		RhO_2	-0.02
	OsO_2	-0.03		OsO_2	-0.03
	IrO_2	0.05		IrO_2	0.11
Mo	CrO_2	-0.35	Ru	CrO_2	-0.17
	MnO_2	-0.47		MnO_2	-0.25
	RuO_2	-0.12		MoO_2	0.03
	RhO_2	-0.45		RhO_2	-0.41
	OsO_2	-0.28		OsO_2	-0.31
	IrO_2	-0.27		IrO_2	-0.21
Rh	CrO_2	0.19	Os	CrO_2	0.05

	MnO_2	0.16		MnO_2	-0.16
	MoO_2	0.33		MoO_2	0.30
	RuO_2	0.34		RuO_2	0.22
	OsO_2	-0.03		RhO_2	-0.27
	IrO_2	0.14		IrO_2	0.04
Ir	CrO_2	-0.01			
	MnO_2	-0.04			
	MoO_2	0.28			
	RuO_2	0.19			
	RhO_2	-0.22			
	OsO_2	-0.11			

Reference

1. Kresse, G.; Hafner, J., Ab initio molecular-dynamics simulation of the liquid-metal-amorphous-semiconductor transition in germanium. *Phys. Rev. B* **1994**, *49* (20), 14251-69.
2. Kresse, G.; Furthmuller, J., Efficiency of ab-initio total energy calculations for metals and semiconductors using a plane-wave basis set. *Comp. Mater. Sci.* **1996**, *6* (1), 15-50.
3. Kresse, G.; Joubert, D., From ultrasoft pseudopotentials to the projector augmented-wave method. *Phys. Rev. B* **1999**, *59* (3), 1758.
4. Yuan, H.; Sun, N.; Chen, J.; Jin, J.; Wang, H.; Hu, P., Insight into the NH_3-Assisted Selective Catalytic Reduction of NO on β-MnO_2 (110): Reaction Mechanism, Activity Descriptor, and Evolution from a Pristine State to a Steady State. *ACS Catal.* **2018**, *8* (10), 9269-9279.
5. Mellan, T. A.; Maenetja, K. P.; Ngoepe, P. E.; Woodley, S. M.; Catlow, C. R. A.; Grau-Crespo, R., Lithium and oxygen adsorption at the β-MnO_2 (110) surface. *J. Mater. Chem. A* **2013**, *1* (47), 14879-14887.
6. Rossmeisl, J.; Qu, Z.-W.; Zhu, H.; Kroes, G.-J.; Nørskov, J. K., Electrolysis of water on oxide surfaces. *J. Electroanal. Chem.* **2007,** *607* (1-2), 83-89.
7. Valdes, A.; Qu, Z.-W.; Kroes, G.-J.; Rossmeisl, J.; Nørskov, J. K., Oxidation and photo-oxidation of water on TiO2 surface. *J. Phys. Chem. C* **2008,** *112* (26), 9872-9879.
8. Liao, P.; Keith, J. A.; Carter, E. A., Water oxidation on pure and doped hematite (0001) surfaces: Prediction of Co and Ni as effective dopants for electrocatalysis. *J. Am. Chem. Soc.* **2012,** *134* (32), 13296-13309.
9. Bajdich, M.; García-Mota, M.; Vojvodic, A.; Nørskov, J. K.; Bell, A. T., Theoretical investigation of the activity of cobalt oxides for the electrochemical oxidation of water. *J. Am. Chem. Soc.* **2013,** *135* (36), 13521-13530.
10. Friebel, D.; Louie, M. W.; Bajdich, M.; Sanwald, K. E.; Cai, Y.; Wise, A. M.; Cheng, M.-J.; Sokaras, D.; Weng, T.-C.; Alonso-Mori, R., Identification of highly active Fe sites in (Ni, Fe) OOH for electrocatalytic water splitting. *J. Am. Chem. Soc.* **2015,** *137* (3), 1305-1313.